Phosphorylation Mutants Elucidate the Mechanism of Annexin IV-Mediated Membrane Aggregation[†,‡]

M. A. Kaetzel,[§] Y. D. Mo,[||] T. R. Mealy,[||] B. Campos,[§] W. Bergsma-Schutter,[⊥] A. Brisson,[⊥] J. R. Dedman,[§] and B. A. Seaton*,[||]

Departments of Molecular and Cellular Physiology and of Obstetrics and Gynecology, University of Cincinnati, College of Medicine, 231 Bethesda Avenue, Cincinnati, Ohio 45220, Department of Physiology and Biophysics, Boston University School of Medicine, 715 Albany Street, Boston, Massachusetts 02118, and Department of Biophysical Chemistry, GBB, University of Groningen, Nijenborgh 4, 9747AG Groningen, The Netherlands

Received October 30, 2000; Revised Manuscript Received January 26, 2001

ABSTRACT: Site-directed mutagenesis, electron microscopy, and X-ray crystallography were used to probe the structural basis of annexin IV-induced membrane aggregation and the inhibition of this property by protein kinase C phosphorylation. Site-directed mutants that either mimic (Thr6Asp, T6D) or prevent (Thr6Ala, T6A) phosphorylation of threonine 6 were produced for these studies and compared with wild-type annexin IV. In vitro assays showed that unmodified wild-type annexin IV and the T6A mutant, but not PKC-phosphorylated wild-type or the T6D mutant, promote vesicle aggregation. Electron crystallographic data of wild-type and T6D annexin IV revealed that, similar to annexin V, the annexin IV proteins form 2D trimer-based ordered arrays on phospholipid monolayers. Cryo-electron microscopic images of junctions formed between lipid vesicles in the presence of wild-type annexin IV indicated a separation distance corresponding to the thickness of two layers of membrane-bound annexin IV. In this orientation, a single layer of WT annexin IV, attached to the outer leaflet of one vesicle, would undergo face-to-face self-association with the annexin layer of a second vesicle. The 2.0-Å resolution crystal structure of the T6D mutant showed that the mutation causes release of the N-terminal tail from the protein core. This change would preclude the face-to-face annexin self-association required to aggregate vesicles. The data suggest that reversible complex formation through phosphorylation and dephosphorylation could occur in vivo and play a role in the regulation of vesicle trafficking following changes in physiological states.

Annexins are a family of structurally related eukaryotic proteins characterized by the property of binding, or annexing, anionic phospholipid membranes in a calcium-dependent manner. This property underlies most of their proposed biological functions, which include vesicular transport, exocytosis and endocytosis, and interactions between membranous and cytoskeletal elements (*1*−*6*). Cells contain multiple annexins, and family members may exert specialized regulatory influence on membrane processes. For example, transport and insertion of membrane components into a functional site provides a mechanism for rapid response to changes in the physiological state. This process can be rapidly reversed through endocytosis or sequestration of plasma membrane domains as vesicles in the cytoplasm. Several annexins including I, II, and IV, when membrane-bound, aggregate phospholipid-containing vesicles prior to fusion, while others, including annexin V, do not promote aggregation. Phosphorylation of aggregation-promoting annexins has an inhibitory effect on that property (for review, see *7*). The present study focuses on the effects of phosphorylation by protein kinase C (PKC)[1] on membrane aggregation mediated by annexin IV. This 35-kDa annexin is abundant in many tissues, where it localizes to the apical membrane of epithelial cells (*8*−*10*). Annexin IV has been associated with the regulation of chloride ion efflux from these cells in culture (*11*, *12*).

The ability of annexins to aggregate membranes has been localized primarily to the N-terminal region, which also contains the major phosphorylation sites. Annexins share a common structural organization comprised of a highly conserved "core" region, which binds calcium ions and phospholipid membranes, and an N-terminal "tail" region that varies in both length and sequence. Chimeric proteins comprised of annexin I N-terminal residues and the C-

[†] This work was supported by the NIH (DK-41740 to M.A.K., DK-46433 to J.R.D., GM-44554 to B.A.S.), the American Heart Association (9930171N to B.C.), the EU (BIO4CT96−0083 to A.B.), and The Caroline Halfter Spahn Trust (to J.R.D. and M.A.K.).

[‡] Coordinates have been deposited in the Protein Data Bank, accession number 1I4A.

* To whom correspondence should be addressed: 617-638-5061 (tel); 617-638-4273 (fax); seaton@med-xtal.bu.edu (e-mail).

[§] University of Cincinnati.

[||] Boston University School of Medicine.

[⊥] University of Groningen.

[1] Abbreviations: NBD-PS, 1-oleoyl-2-[12-[(7-nitro-2,1,3-benzoxadiazol-4-yl)amino]dodecanoyl]-*sn*-glycero-3-phosphoserine; T6D, Thr6→Asp site-directed mutant; T6A, Thr6→Ala site-directed mutant; PS, phosphatidylserine; DOPS, dioleoylphosphatidylserine; DOPC, dioleoylphosphatidylcholine; HEPES, *N*-(2-hydroxyethyl)piperazine-*N*′-2-ethanesulfonic acid; HEPPS, *N*-(2-hydroxyethyl)piperazine-*N*′-2-propanesulfonic acid; PKC, protein kinase C; EGTA, ethylene glycol bis(*β*-aminoethyl ether)-*N*,*N*,*N*′,*N*′-tetraacetic acid.

10.1021/bi002507s CCC: $20.00
Published on Web 03/08/2001

terminal core of annexin V possess the ability to aggregate membranes, a property of annexin I but not annexin V (*13*−*15*). The detailed mechanism of membrane aggregation by annexins is unclear, though several models have been proposed (*16*). Cryo-EM studies of annexin−membrane junctions (*17*) have shown that annexin-binding accessory proteins, such as the p11 component of the annexin II heterotetramer, can be involved in coupling two membrane-bound layers of annexins. Yet junctions also form in the absence of these accessory proteins, proving that the annexin structure is sufficient in itself to aggregate membranes. The ability to self-associate into extended ordered arrays on phospholipid monolayer surfaces (2D crystallization), which has been visualized for annexins V (*18, 19*) and VI (*20, 21*), may be part of this process. However, to date, this crystallization behavior has not been documented for any annexins that promote membrane aggregation. Neither annexin I nor annexin II has been observed to form trimer-based arrays as does annexin V (A. Brisson, unpublished observations). The annexin−liposome junction studies by cryo-EM show that annexin-coated membrane surfaces participate in formation of these junctions. Although this observation suggests the stabilizing role of protein−protein interactions, it was not proven that true 2D-ordered arrays were formed under these conditions.

The crystal structure of wild-type bovine annexin IV has been determined (*22, 23*). The ability of annexin IV to self-associate on membrane surfaces also has been reported (*24*), though not in the form of 2D crystals. Annexin IV has been shown to aggregate synthetic phospholipid vesicles and chromaffin granules (*24*−*26*), but as yet no accessory protein has been identified. Annexin IV is phosphorylated by PKC but not calmodulin-dependent kinase II, protein kinase A, or tyrosine kinases. The major site for annexin IV phosphorylation is Thr6, whereas the PKC sites in annexins I and II are concentrated in the N-terminal tail regions that are not common with annexin IV (*7*). Site-directed mutagenesis studies of annexins I and II have demonstrated that substitution of acidic residues at the PKC sites mimics phosphorylation and can have a negative effect on properties such as annexin II/p11 association and annexin-induced membrane aggregation (*27*−*29*). In the present study, site-engineered mutants of annexin IV were used to study the consequences of PKC phosphorylation at Thr6. X-ray crystallographic and electron microscopic analyses were performed on wild-type and mutant annexin IV proteins to evaluate the effects of phosphorylation on annexin structure, self-association, and formation of inter-liposome junctions during membrane aggregation.

MATERIALS AND METHODS

Recombinant Annexin Proteins. Plasmid pMNEndo1 within *E. coli* strain BL21DE3 was kindly provided by Carl E. Creutz, University of Virginia. The bovine annexin IV (Endo1) cDNA was excised from the pET11d vector with *Nco*I and *Eco*RI, and was inserted into the plasmid pKK233-2 (Pharmacia Biotech). The Transformer Site-Directed Mutagenesis Kit (Clontech) was used to convert threonine 6 (ACT) to alanine (GCT) or aspartic acid (GAT). Correct base changes to yield T6A and T6D were verified by double-strand DNA sequence analysis. Mutated annexin IV inserts were excised and religated into pET11d for protein expression.

E. coli BL21DE3 harboring pET11d annexin IV (*30, 31*) were induced to express protein with 0.4 mM isopropyl β-D-thiogalactopyranoside after exponential growth was monitored by the optical density of 0.6 at 600 nm. After 3 h, bacteria were harvested by centrifugation. Pellets were resuspended in 50 mM HEPES (pH 7.3) buffer containing 150 mM NaCl and 5 mM EDTA and were stored at −80 °C. Soluble protein was released from bacteria by thawing in the presence of 2 mg/mL lysozyme and sonicating 3 times for 20 s. Particulate material was removed by centrifugation at 10000*g* for 30 min. Annexin IV was purified from the supernatant as previously described (*8*). The sample was dialyzed against a buffer of 20 mM Tris (pH 7.4), 1 mM EGTA, 0.2 M NaCl, 1 mM magnesium acetate, and 7 mM 2-mercaptoethanol. Calcium was added to achieve a final concentration of 1 mM excess, and the sample was applied to a 30-mL column of phenyl-Sepharose 4B (Pharmacia) coated with bovine brain phospholipid fraction III (Sigma). Column wash buffer (150 mL) contained 1 mM $CaCl_2$. Annexin IV was eluted by chelation of calcium with buffer containing 1 mM EGTA. Annexin IV was further concentrated and purified by Mono Q chromatography (Pharmacia) using a gradient of 0−200 mM NaCl (*32*). Mass spectral analyses of wild-type annexin IV and the T6D and T6A mutants were consistent with the sequences of the respective full-length proteins. Samples were run by electrospray ionization (ESI) on a Micromass (Beverly, MA) Quattro II triple quadrupole tandem mass spectrometer, located at the Boston University School of Medicine Mass Spectrometry Resource. Wild-type rat annexin V was prepared as described previously (*33*).

Annexin IV Phosphorylation by Protein Kinase C. Wild-type annexin IV was phosphorylated with rat brain protein kinase C (Calbiochem). The reaction was performed in 20 mM HEPES buffer (pH 7.4), 2 mM ATP, 10 mM $MgCl_2$, 0.2 mM $CaCl_2$, 0.02% Triton X-100 with sonicated 0.2 mg/mL brain phospholipid and 0.004 mg/mL diacylglycerol as activator. Protein kinase C (1.7 units, phosphorylating 1.7 nmol/min) was added to 0.5 mg of annexin IV and incubated at 30 °C for 30 min. EGTA was added at a final concentration of 5 mM excess chelator to release annexin IV from phospholipid. Phospholipid was removed by centrifugation at 100000*g* for 30 min. The supernatant was dialyzed against 50 mM HEPES (pH 7.4), 100 mM KCl, 0.1 mM DTT, and 0.1 mM EGTA for further studies. Protein concentrations were determined using Coomassie Plus Protein Assay Reagent (Pierce) using bovine serum albumin as a standard.

Liposome Preparation. Liposomes used for the aggregation assays were composed of 1:1 mixtures of DOPS/DOPC (Avanti Polar Lipids), and were prepared by drying lipid/chloroform solutions by rotary evaporation and suspension in buffer (0.1 M KCl, 50 mM HEPES, pH 7.4, 0.02% NaN_3, 0.1 mM DTT) to a final concentration of 5 mM. The lipid suspensions were extruded through an Avestin 100-nm membrane pore size LiposoFast homogenizer 19−21 times. The final phospholipid concentrations were determined by a phosphate ashing procedure (*34*). Liposomes used for cryo-EM were prepared as described previously (*17*), using DOPC and DOPG from Avanti Polar Lipids. *N*-Octyl-β-D-glucopyranoside (β-OG) and *N*-(2-hydroxyethyl)piperazine-*N*′-3-

propanesulfonic acid (HEPPS) were from Sigma. Liposomes were prepared by detergent dialysis (*35, 36*), as follows. Appropriate volumes of chloroform solutions were mixed which correspond to 1 mg of DOPG, 4 mg of DOPC, and 25 mg of β-OG. After evaporation of the chloroform, lipids were resuspended in 100 mM KCl, 3 mM NaN_3, 25 mM HEPPS, pH 8.0, at a final lipid concentration of 5 mg/mL. The mixture was allowed to stand for 1 h at room temperature and was then poured into Spectra/Por no. 1 dialysis tubing (Medicell Int., London, U.K.) with a molecular mass cutoff of 6000−8000 Da. Dialysis was performed at ambient temperature for 2 days against a bath containing 500 mL of the same buffer, with an exchange of the dialysis solution after 1 day.

Liposome Aggregation Assays. Aggregation of liposomes by annexin IV was determined from the change in absorbance following the increase in turbidity of the liposome suspension (*37*). Absorbance was measured at 350 nm in a Perkin-Elmer Lambda 2 spectrophotometer. Data were collected and recorded at discrete intervals. The experiments were carried out in 1-cm quartz cuvettes at room temperature. The standard assay was conducted for 3 min in 300 mM sucrose, 40 mM HEPES buffer, pH 7.4, in the presence of 1 mM $CaCl_2$, 0.5 mM $MgCl_2$, and 10 μg of protein. To initiate the reaction, an aliquot of the vesicles was added to give a final vesicle concentration of 80 μM.

Ca^{2+}-Dependent Phospholipid Binding. Annexin IV proteins, wild type, wild type phosphorylated by PKC, mutant T6D, and mutant T6A, were assessed for Ca^{2+}-dependent binding to artificial membrane vesicles. Phosphatidylserine (Sigma B-1627) containing vesicles were prepared according to Hamman et al. (*30*). The vesicles (400 μL, 1 mg/mL) were pelleted at 18 psi for 15 min in a Beckman airfuge. Four pellets were resuspended individually with 0.1 mg of the four annexin IV isoforms in 200 μL of a buffer containing 10 mM Tris (pH 7.4), 1 mM EGTA, 2 mM $CaCl_2$, and 150 mM NaCl and centrifuged at 18 psi for 15 min. The resulting supernatants were withdrawn, and the pellets were resuspended in buffer containing 1 mM EGTA but no added $CaCl_2$. The suspensions were centrifuged at 18 psi for 15 min. The initial protein samples, the Ca^{2+}-containing supernatants, and the proteins eluted by chelation of Ca^{2+} were treated with SDS-sample buffer (90 °C for 5 min), separated by SDS−PAGE (12% gel; NOVEX), and stained with Coomassie blue.

The half-maximal Ca^{2+} dependence of annexin binding to liposomes was estimated using a vesicle sedimentation protocol described previously (*33*). Briefly, samples of annexin and phospholipid vesicles were incubated together at a range of $CaCl_2$ concentrations and subsequently centrifuged for 45 min at 1000*g* through a Centricon filtering device. Washed retentates and filtrates were subjected to SDS−PAGE. Relative band intensities were measured to assess the $CaCl_2$ concentration at which half-maximal binding of annexin to liposomes occurred.

Crystallographic Analysis of Annexin IV Mutants. Recombinant bovine T6D annexin IV was crystallized at 17 °C by vapor diffusion against a reservoir of 20−35% saturated ammonium sulfate, 100 mM sodium acetate, pH 5.0, 0.02% sodium azide, 2 mM dithiothreitol, and 10 mM $CaCl_2$. Final protein and calcium concentrations at equilibrium were 14 mg/mL and 20 mM, respectively. X-ray data were collected to 2.0-Å resolution at the Brookhaven National Laboratory Synchrotron and were processed and scaled using DENZO and SCALEPACK (*38*) (Table 1). The structure was solved by molecular replacement, using AMoRe (*39*). Crystals of T6D annexin IV are isomorphous with the *R3* crystals of the wild-type annexin IV structure reported at 3-Å resolution (*23*). However, a search model obtained from a wild-type annexin IV structure solved to 2.3-Å resolution in a $P2_1$ unit cell (*22*) (Protein DataBank accession no. 1ANN), gave the best molecular replacement solution. Model-building and refinement were carried out using O (*40*) and CNS (*41*), respectively. Iterative cycles of manual rebuilding, refinement, and calculation of difference and simulated-annealing omit maps improved the model to its final form. Data collection and refinement statistics are presented in Table 1.

Table 1: Crystallographic Data and Refinement Statistics

Crystallographic Data	
space group	*R3*
cell dimensions (Å)	$a = 119.055$, $c = 82.157$
resolution range (Å)	100−2.0
no. of unique reflections, theoretical (obsd)	29310 (28686)
redundancy (highest resolution shell)[a]	2.00 (1.97)
completeness (%) (highest resolution shell)[a]	97.9 (99.2)
R_{merge} (highest resolution shell)[a,b]	0.065 (0.124)
average $I/\sigma I$ (highest resolution shell)[a]	16.9 (9.0)
Model Refinement	
applied resolution limit (Å)	2.0
no. of reflections used in refinement	28309
no. of non-H atoms	2975
no. of calcium ions	2
no. of sulfate ions	1
no. of water molecules	256
R_{cryst}[c]	0.2094
R_{free}[d]	0.2324
rmsd,[e] bond	
lengths (Å)	0.005971
angles (deg)	1.12117
average *B*-factor (Å^2)	27.3586
minimum *B*-factor (Å^2)	12.3631
maximum *B*-factor (Å^2)	68.8731

[a] Values taken from output of SCALEPACK (*38*). [b] $R_{merge} = \Sigma|I_i - \langle I\rangle|/\Sigma I_i \times 100$ where I_i is the intensity of an individual reflection and $\langle I\rangle$ is the mean intensity of that reflection. [c] $R_{cryst} = \Sigma||F_p| - |F_{calc}||/\Sigma|F_p| \times 100$ where $|F_{calc}|$ is the calculated structure factor. [d] R_{free} is as defined by Brünger (*51*). [e] rmsd = root-mean-square deviation.

Electron Crystallography of Annexin IV 2D crystals. The experimental conditions used for growing 2D crystals of both wild-type and T6D annexin IV on lipid monolayers were similar to those described in detail for annexin V (*42, 43*). Briefly, 17 μL of a 0.2 mg/mL protein solution in 2 mM Ca^{2+}, 150 mM NaCl, 10 mM HEPES, 3 mM NaN_3, pH 7.4, was deposited in a Teflon well, and 0.6 mL of a lipid solution containing 150 mM DOPS/450 mM DOPC in chloroform/hexane (1:1, v/v) was deposited on top of it. After overnight incubation at ambient temperature in a humid chamber, the crystalline material present at the air−water interface was transferred onto a 400-mesh EM grid coated with a perforated carbon film, and negatively stained with 1% uranyl acetate, pH 3.5. Electron microscopy was carried out with a Philips CM120 operating at 120 kV, equipped with a 1k × 1k Gatan-794 slow-scan CCD camera. A semi-automated procedure was used for selecting the areas of best crystalline quality (*44*). Electron images were recorded under low-dose conditions at 44000× magnification. Image processing was

performed using standard crystallographic methods based on a suite of MRC and modified IMAGIC programs.

Cryo-EM of Intermembrane Junctions Formed between Annexin IV and Liposomes. DOPG/DOPC liposomes (25 μg; weight ratio 1:4) were mixed with either wild-type annexin IV (30 μg) or mutant T6D (30 μg) in a buffer containing 1 mM $CaCl_2$, 100 mM NaCl, 30 mM KCl, 3 mM NaN_3, 25 mM HEPES, pH 7.4, at ambient temperature. Liposomes were prepared as described above. After 15 min incubation, a few microliters of the mixture was deposited on an EM grid coated with a perforated carbon film, and the grid was quickly plunged into liquid ethane, according to standard cryo-EM procedures (*45*). Grids were mounted in a Gatan-626 cryo-holder (Warrendale, PA), and subsequent EM observations were made at −170 °C. Images were recorded at 44000× magnification and 1-μm underfocus with a slow-scan CCD camera. Density profiles of selected junctions were calculated as described in (*17*). The overall thickness of the junction was measured at the mid-position along the density profile, between maxima and minima, as calculated for other annexin-induced junctions (*17*).

RESULTS

Liposome Binding and Aggregation. Native and phosphorylated wild-type annexin IV proteins and the T6D and T6A mutant annexin IV proteins were evaluated for the ability to bind and aggregate synthetic liposomes. Liposome sedimentation assay results confirmed that all the protein samples bound to the PS-containing vesicles in a Ca^{2+}-dependent manner (Figure 1a). In a buffer containing 1 mM free Ca^{2+}, all four proteins appeared in the pellet following centrifugation, indicating that they were fully bound to the vesicles. The proteins in these samples were completely eluted from the vesicles after resuspending them in a Ca^{2+}-free buffer (i.e., 1 mM EGTA with no added Ca^{2+}) and submitting them again to centrifugation, whereupon they appeared in the supernatant. The half-maximal Ca^{2+} concentration for annexin−membrane binding, as measured by the liposome sedimentation assay (*33*), was found to be at least 2 orders of magnitude less than the millimolar Ca^{2+} concentrations used in the structural experiments (data not shown). Therefore, the reported data reflect the properties of the membrane-bound proteins.

In liposome aggregation assays, WT and T6A annexin IV both induced aggregation to a comparable extent, while phosphorylated wild-type, T6D mutant annexin IV (Figure 1b), or a negative control, annexin V (data not shown), exhibited no aggregation. To determine whether phospholipid composition had an effect on aggregation, vesicles composed of a 1:1 mixture of DOPC and either brain or synthetic DOPS were incubated with the different annexin samples and assayed for aggregation. Vesicles containing brain or synthetic PS, or DOPA or DOPG instead of PS, gave the same results (data not shown), indicating that the aggregation was not sensitive to these differences in vesicle composition.

2D Electron Crystallography and Cryo-Electron Microscopy. Two different electron microscopy (EM) approaches were used to investigate the structure of complexes formed between wild-type or T6D annexin IV and lipid membranes. First, both proteins were shown to self-organize into 2D crystals by specific binding to lipid monolayers. The crystals

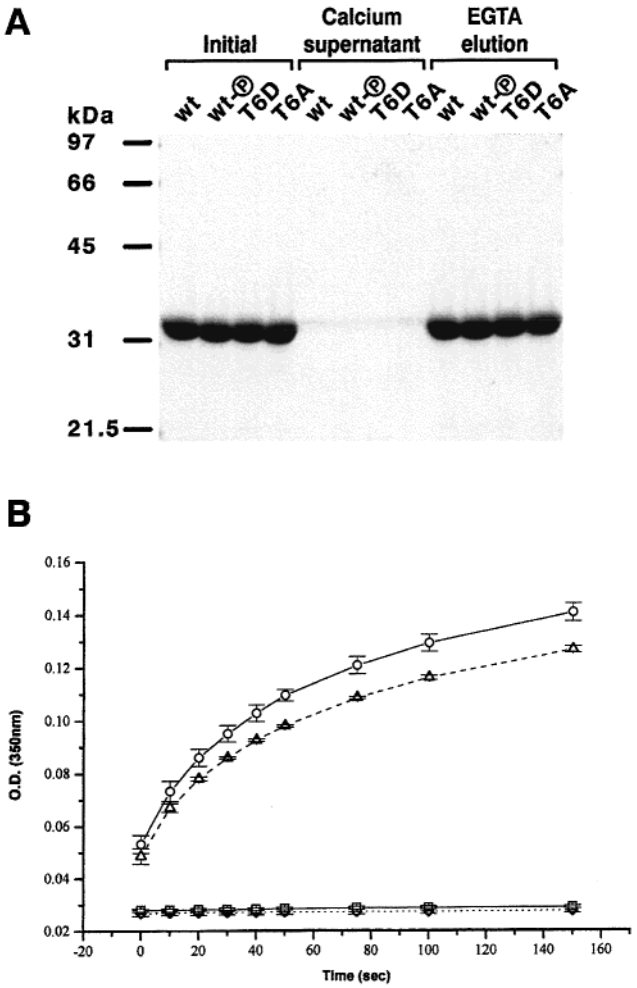

FIGURE 1: (a) SDS−PAGE analysis of Ca^{2+}-dependent reversible binding of annexin IV to PS-containing vesicles incubated with wild-type annexin IV (WT), wild-type phosphorylated by PKC (WT-P), or mutants T6D or T6A. (Lanes 1−4) Annexin IV−vesicle samples at 1 mM free Ca^{2+}. (Lanes 5−8) Supernatant collected following centrifugal sedimentation of annexin IV−vesicle samples at 1 mM free Ca^{2+}. (Lanes 9−12) Pellet collected following sedimentation of annexin IV−vesicle samples at 1 mM free Ca^{2+}, followed by resuspension and resedimentation in Ca^{2+}-free buffer. (b) Spectrometric assay of aggregation of brain PS/DOPC (1:1) liposomes by annexin IV wild-type (circles), T6A mutant (triangles), T6D mutant (diamonds), or phosphorylated wild-type annexin IV (squares).

formed by wild-type and T6D annexin IV are almost identical and consist of annexin IV trimers packed with *p3* symmetry, as shown in Figure 2 for wild-type annexin IV. This ordered assembly of trimers is reminiscent of that exhibited by annexin V (*42*). Second, cryo-EM was used to study the structure of complexes formed between liposomes and either wild-type annexin IV or mutant T6D. In the presence of wild-type annexin IV, liposomes were found to be tightly associated via characteristic junctions (Figure 3a). At the level of the junctions, adjacent liposomes exhibit almost flat surfaces, indicating that the collective effect of membrane-bound annexin IV molecules is strong enough to alter the natural spherical curvature of the liposomes. The junctions occur with a continuous width of 17 ± 0.5 nm and a consistent morphology, with the outer lipid leaflet being significantly thicker than the inner lipid leaflet and often exhibiting a particulate pattern. The mixtures of DOPC/

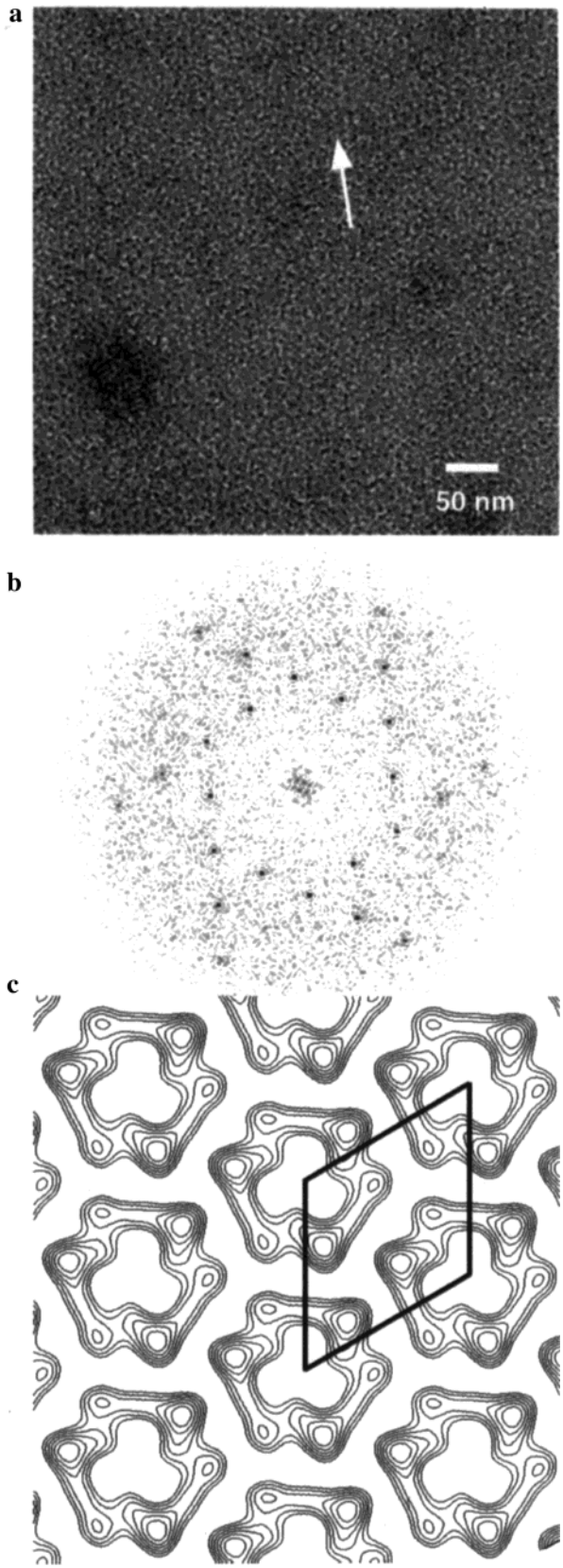

FIGURE 2: (a) Image 512 × 512 of a crystalline domain of membrane-bound annexin IV, negatively stained. Parallel striations are observed along the direction of the arrow. (b) Fourier transform of image (a). Diffraction peaks, located on a hexagonal lattice, extend up to a resolution of 2.5 nm. (c) 2D projection map calculated from image (a), after *P3* symmetrization. The triangular motifs correspond to trimers of annexin IV. The unit cell dimensions are $a = b = 105$ Å, $\gamma = 120°$. Protein densities are represented as contours.

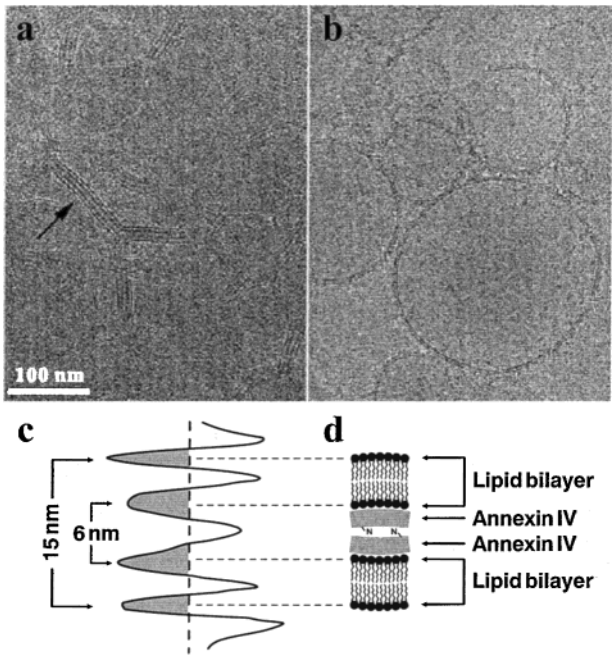

FIGURE 3: (a) Cryo-electron micrograph of intermembrane junctions induced by wild-type annexin IV. The junctions connect the liposomes into a dense 3D network. (b) Cryo-electron micrograph of a mixture of liposomes and T6D mutant. No junctions are observed. (c) Profile of projected density of the junction shown in (a) with an arrow. Shaded peaks to the left of the vertical dashed line represent density maxima corresponding to the centers of mass of the structural elements, e.g., the inner and outer leaflets of the vesicles. Distance measurements are between maxima; the thickness of the junction is slightly greater as it is measured at the mid-position along the density profile, between maxima and minima, as in (*17*). (d) Model of an annexin IV-induced junction.

DOPG liposomes and mutant T6D presented a totally different appearance (Figure 3b). Isolated liposomes were observed, which appeared almost identical to pure liposomes (not shown), with the two lipid layers well resolved, separated by about 5 nm with no flattened surface. The presence of bound annexin T6D molecules could be detected by the presence of a poorly contrasted layer of material protruding at the outer surface of the liposomes.

Three-Dimensional Crystallographic Analysis of T6D Annexin IV. Comparison of the T6D and wild-type annexin IV crystal structures shows that the two molecular structures are quite similar: the root-mean-square-deviation in domain I, where the mutation occurs, is only 0.38 Å^2. Conformational differences between the two structures are evident in only two locations, the N-terminus and one of the calcium-binding loops (Figure 4). Electron density is not observed for residues 1−9 in the T6D mutant crystal structure. Mass spectral data rule out truncation of the N-terminus in these crystals, indicating that these residues are present but disordered, unlike the WT protein (see Discussion). In the T6D mutant structure, the position of the IIIAB loop is in a more exposed conformation than in the wild-type, and the Trp185 side chain does not adopt a buried conformation. This conformational difference appears to be related to differences in lattice packing in the two crystal forms ($P2_1$ and $R3$). Two Ca^{2+} ions are observed in the AB (i.e., between the A and B helices) Ca^{2+}-binding loops of domains I and IV. These are coordinated similarly in the WT and T6D annexin IV structures.

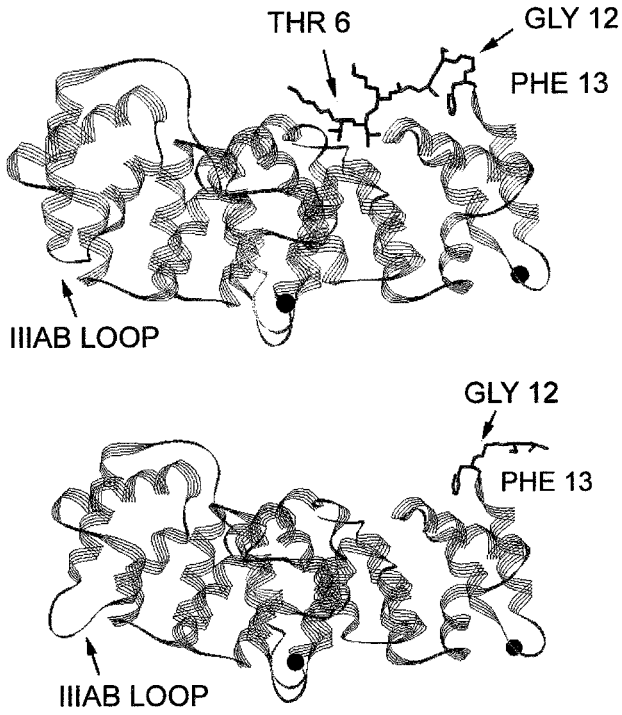

FIGURE 4: Ribbon diagrams of annexin IV crystal structures. (Top) Wild-type (*22*). (Bottom) T6D mutant. Calcium ions are shown as dark spheres in the IAB (right) and IVAB (left) loops. Figure prepared in Swiss-PDB Viewer (*50*).

DISCUSSION

Annexins have been widely implicated in membrane trafficking (*5*) and are abundant in cellular locations such as chromaffin secretory granules, which can undergo annexin-mediated aggregation prior to fusion. Little is known on a molecular level regarding the mechanism of annexin-mediated membrane aggregation. Current knowledge is derived primarily from systems in which the annexin is assisted by an accessory protein. The best-characterized example is the annexin II tetramer (aIIt), which is composed of two molecules of annexin II and two molecules of the accessory protein, p11 (*46*). This 11-kDa protein, like the accessory proteins binding to annexins I (*47*), VII (*48*), and XI (*49*), belongs to the S-100 family of E-F hand proteins. The principal binding sites for these smaller proteins are located within the annexin N-terminal domain. Cryo-images of aIIt−liposome junctions show distinct "stripes" of electron density, which correspond to the inner and outer leaflets of one vesicle, an annexin II layer, a p11 layer, another annexin II layer, and the two leaflets of the apposing vesicle (*17*). Phosphorylation may interfere with formation of the central p11 layer by disrupting annexin II−p11 binding sites within the annexin N-terminal domain (*29*). What is unclear from the above model is how membrane aggregation can occur in the absence of accessory proteins, as observed for annexin IV. In cryo-EM images of lipid junctions in the presence of annexins I or II alone, the central electron-dense "stripe" corresponding to the accessory protein is absent, and the junctions themselves are of lesser thickness than those induced by the aIIt tetramer. Therefore, the bridging must be of a somewhat different structural organization and, in the former case, accomplished solely through the annexin molecules.

The cryo-EM images shown in Figure 3 are taken from frozen-hydrated, unstained specimens, which allows complex macromolecular assemblies to be viewed in a near-native environment. These data permit a detailed structural analysis of the lipid junctions induced by annexin IV. In the density profile shown in Figure 3c, the maxima correspond to the centers of mass of the more strongly scattering structural elements, while the positions of the minima delineate the boundary of these elements. The maxima in the density profile correspond to the dark stripes in the image in Figure 3a. The junctions formed in the presence of WT annexin IV present four dark layers of electron scattering matter, with the two central ones being thicker/more dense than the outer ones. These two outer stripes correspond to the inner leaflets of the liposomes involved in the junction. The two thicker central stripes correspond to the two protein-bound outer leaflets, where the protein layer is unresolved from the membrane leaflet but contributes to the total scattering (Figure 3c,d). In contrast, images of pure liposomes show only two dark stripes, where the outer leaflet is considerably thinner than that of the central stripes in the junction (data not shown). Images of liposomes with bound annexin V, under conditions of 100% surface coverage, present an intermediate appearance between pure liposomes and annexin IV-covered liposomes (*17*). Annexin V does not induce junction formation, but its coating of the membrane surface presents a rough appearance. The overall thickness of the membrane is about 7.5−8.0 nM, which is about that of one layer of annexin bound to one lipid bilayer (*17*). The cryo-EM image of liposomes in the presence of T6D annexin IV, shown in Figure 3b, is very similar to that of annexin V. Here again, the outer leaflet is coated with the annexin mutant, but no junctions are observed. The protein layer adds to the scattering of the vesicle outer leaflet and can be detected as faint protrusions on the otherwise smooth lipid layer.

In the present studies, the overall thickness of the WT annexin IV-mediated junctions, approximately 17 nm, is similar to that of vesicle junctions formed by either annexin I or annexin II (*17*). This indicates that the basic molecular structure of the junctions induced by annexin IV, annexin I, or annexin II is very similar. Crystal structures show that the thickness of the annexin core domain is approximately 30 Å from the convex to the concave sides of the molecule. In the cryo-EM image of the annexin IV-induced junction, the two outer leaflets are separated by 60 Å, the thickness of two annexin molecules. Given that the annexin convex face, which contains the Ca^{2+}/membrane-binding sites, must be oriented toward the bilayer, the concave face must be the one to participate in the face-to-face self-association. These data cannot address whether actual dimer formation takes place between annexin monomers on different liposomes. Rather, the evidence indicates only that the membrane-bound layer of annexin molecules must be oriented with the concave surfaces facing outward. Since the monomers form extended, single-layer arrays on each leaflet, it seems equally likely that the two surfaces interdigitate via the concave annexin faces, but this remains undetermined.

Phosphorylation at the N-terminus may inhibit membrane aggregation by altering the face-to-face self-association of membrane-bound annexin IV. The X-ray crystallographic data described herein suggest that the conformation of the

N-terminus of wild-type annexin IV is significantly affected by phosphorylation. In the 2.3-Å resolution crystal structure of wild-type bovine annexin IV, the N-terminus lacks the first three residues (Ala-Ala-Lys), which are too mobile to be observed (*22*). The remaining N-terminal residues, 4−14, form an irregular, extended secondary structure resembling a single strand of β-sheet. This strand lies across the concave protein surface. The side chains of Thr6, Val7, and Phe13 participate in hydrophobic interactions that help anchor the N-terminal strand to the C-terminal core domain. Introduction of a negative charge at position 6 would be expected to weaken these interactions and destabilize this anchored portion of the N-terminal region (*22*). The crystal structure of T6D annexin IV confirms that with the introduction of aspartate at this position, the first 11 N-terminal residues are released from the annexin core (Figure 4). This change occurs without any perturbation of the C-terminal core structure. The Phe13 side chain remains anchored to the core, while Gly12 serves as a hinge to permit the conformational change to take place.

From the combined studies, the following model is proposed to explain the homotropic (i.e., without accessory proteins) mode of annexin IV-mediated membrane aggregation. Annexin IV molecules bind to the liposome surfaces and form extensive well-ordered arrays that coat the membrane leaflet with a single annexin layer. Two such leaflets approach each other, and their annexin layers interact face-to-face. Thus, the membrane-bound annexin layers form self-adhesive sheets that form the nexus between adjacent vesicles. N-terminal phosphorylation changes the local protein conformation so that the facing annexin sheets cannot interact with each other, and membrane aggregation does not occur. This model predicts that the assembly process could be reversible following dephosphorylation. With the negatively charged phosphoryl group removed from Thr6, the N-terminal strand would be free to return to its binding crevice to adopt its native conformation, which in turn would permit productive annexin−annexin complexes to form at the concave surfaces, leading to vesicle aggregation. From this model, phosphorylation would not be expected to remove the annexin layer from the membrane, since the membrane-binding and structural properties associated with the annexin core are not significantly affected by phosphorylation. However, it is possible that in the phosphorylated state, annexin IV might be able to mediate cellular functions other than membrane aggregation, and these may operate through alternate mechanisms.

Annexin IV has been shown to regulate Cl^- efflux from cultured epithelial cells by inhibiting calmodulin-dependent protein kinase II-activated Cl^- currents (*11*, *12*). The present data support the possibility that physiologically, annexin IV may play a role in intracellular vesicle trafficking by promoting membrane aggregation in response to an elevated Ca^{2+} transient. Specifically, annexin IV may promote nexus formation between the plasma membrane and vesicles that have been targeted to the cellular domains associated with Cl^- efflux. Phosphorylation of annexin IV by PKC would attenuate the cellular response by preventing further membrane−membrane interactions.

ACKNOWLEDGMENT

We thank F. Oling and W. Keegstra for their help with electron image processing, J. Head for assistance with X-ray data collection, and C. Creutz for providing the annexin IV clone.

REFERENCES

1. Creutz, C. E. (1992) *Science 258*, 924−931.
2. Raynal, P., and Pollard, H. B. (1994) *Biochim Biophys. Acta 1197*, 63−93.
3. Kaetzel, M. A., and Dedman, J. R. (1995) *News Physiol. Sci. 10*, 171−176.
4. Seaton, B. A., Ed. (1996) in *Annexins: molecular structure to cellular function*, 245 pp, R. G. Landes Company, Austin, TX.
5. Gerke, V., and Moss, S. E. (1997) *Biochim Biphys. Acta 1357*, 129−154.
6. Seaton, B. A., and Dedman, J. R. (1998) *Biometals 11*, 399−404.
7. Rothhut, B. (1997) *Cell. Mol. Life Sci. 53*, 522−526.
8. Kaetzel, M. A., Hazarika, P., and Dedman, J. R. (1989) *J. Biol. Chem. 264*, 14463−14470.
9. Kaetzel, M. A., Chan, H. C., Dubinsky, W. P., Dedman, J. R., and Nelson, D. J. (1994) *J. Biol. Chem. 269*, 5297−5302.
10. Mayran, N., Traverso, V., Maroux, S., and Massey-Harroche, D. (1996) *Am. J. Physiol. 270 (5 Pt. 1)*, L863−L871.
11. Chan, H. C., Kaetzel, M. A., Gotter, A. L., Dedman, J. R., and Nelson, D. J. (1994) *J. Biol. Chem. 269*, 32464−32468.
12. Xie, W., Kaetzel, M. A., Bruzik, K. S., Dedman, J. R., Shears, S. B., and Nelson, D. J. (1996) *J. Biol. Chem. 271*, 14092−14097.
13. Ernst, J. D., Hoye, E., Blackwood, R. A., and Mok, T. L. (1991) *J. Biol. Chem. 266*, 6670−6673.
14. Hoekstra, D., Buist-Arkema, R., Klappe, K., and Reutelingsperger, C. P. M. (1993) *Biochemistry 32*, 14194−14202.
15. Bitto, E., and Cho, W. (1999) *Biochemistry 38*, 14094−14100.
16. Meers, P., Mealy, T., Pavlotsky, N., and Tauber, I. A. (1992) *Biochemistry 31*, 6372−6382.
17. Lambert, O., Gerke, V., Bader, M. F., Porte, F., and Brisson, A. (1997) *J. Biol. Chem. 272*, 42−55.
18. Olofsson, A., Mallouh, V., and Brisson, A. (1994) *J. Struct. Biol. 113*, 199−205.
19. Voges, D., Berendes, R., and Burger, A. (1994) *J. Mol. Biol. 238*, 199−213.
20. Benz, J., Bergner, A., and Hofmann, A. (1996) *J. Mol. Biol. 260*, 638−643.
21. Kawasaki, H., Avila-Sakar, A., Creutz, C. E., and Kretsinger, R. H. (1996) *Biochim Biophys. Acta 1313*, 277−282.
22. Sutton, R. B., and Sprang, S. R. (1996) in *Annexins: molecular structure to cellular function* (Seaton, B., Ed.) pp 31−42, R. G. Landes Company, Austin, TX.
23. Zanotti, G., Malpelin, G., Gliubich, F., Folli, C., Stoppini, M., Olivi, L., Savoia, A., and Berni, R. (1998) *Biochem. J. 329*, 101−106.
24. Zaks, W. J., and Creutz, C. E. (1991) *Biochemistry 30*, 9607−9615.
25. Zaks, W. J., and Creutz, C. E. (1990) *Biochim. Biophys. Acta 1029*, 149−160.
26. Blackwood, R. A., and Ernst, J. D. (1990) *Biochem. J. 266*, 195−200.
27. Wang, W., and Creutz, C. E. (1994) *Biochemistry 33*, 275−282.
28. Porte, F., de Santa Barbara, P., Phalipou, S., Liautard, J. P., and Widada, J. S. (1996) *Biochim. Biophys. Acta 1293*, 177−184.
29. Jost, M., and Gerke, V. (1996) *Biochim. Biophys. Acta 1313*, 283−289.
30. Hamman, H. C., Gaffey, L. C., Lynch, K. R., and Creutz, C. E. (1988) *Biochem. Biophys. Res. Commun. 156*, 660−667.
31. Nelson, M. R., and Creutz, C. E. (1995) *Biochemistry 34*, 3121−3132.

32. Seaton, B. A., Head, J. F., Kaetzel, M. A., and Dedman, J. R. (1990) *J. Biol. Chem. 265*, 4567−4569.
33. Campos, B., Mo, Y. D., Mealy, T. R., Li, C. W., Swairjo, M. A., Balch, C., Head, J. F., Retzinger, G., Dedman, J. R., and Seaton, B. A. (1998) *Biochemistry 37*, 8004−8010.
34. Ames, B. N., and Dubin, D. T. (1960) *J. Biol. Chem. 235*, 769−775.
35. Kagawa, H., Tokimatsu, H., and Fukutome, H. (1971) *J. Biochem. (Tokyo) 70*, 225−234.
36. Zumbuehl, O., and Weder, H. G. (1981) *Biochim. Biophys. Acta 640*, 252−262.
37. Lee, G., and Pollard, H. B. (1997) *Anal. Biochem. 252*, 160−164.
38. Otwinowski, Z. (1993) Oscillation Data Reduction Program for Protein Crystallography. in *Proceedings of the CCP4 study weekend: data collection and processing* (Sawyers, L., Isaacs, N., and Bailey, S., Eds.) pp 56−62, SERC Daresbury Laboratory, Warrington, U.K.
39. Navaza, J. (1994) *Acta Crystallogr. A50*, 157−163.
40. Jones, T. A., and Kjeldgaard, M. (1992) *O—The Manual*, Uppsala, Sweden.
41. Brünger, A. T., Adams, P. D., Clore, G. M., DeLano, W. L., Gros, P., Grosse-Kunstleve, R. W., Jiang, J.-S., Kuszewski, J., Nilges, M., Pannu, N. S., Read, R. J., Rice, L. M., Simonson, T., and Warren, G. L. (1998) *Acta Crystallogr., Sect. D D54*, 905−921.
42. Brisson, A., Bergsma-Schutter, W., Oling, F., Lambert, O., and Reviakine, I. (1999) *J. Cryst. Growth 196*, 456−470.
43. Brisson, A., Lambert, O., and Bergsma-Schutter, W. (1999) in *Crystallization of Nucleic Acids and Proteins: A Practical Approach* (Ducruix, A., and Giege, R., Eds.) pp 341−363, Oxford University Press, Oxford, U.K.
44. Oostergetel, G., and Brisson, A. (1998) *Ultramicroscopy 74*, 47−59.
45. Dubochet, J., Lepault, J., Freeman, R., Berriman, J. A., and Homo, J.-C. (1982) *J. Microsc. 128*, 219−237.
46. Waisman, D. M. (1995) *Mol. Cell. Biochem. 149−150*, 301−322.
47. Mailliard, W. S., Haigler, H. T., and Schlaepfer, D. D. (1996) *J. Biol. Chem. 271*, 719−725.
48. Brownawell, A. M., and Creutz, C. E. (1997) *J. Biol. Chem. 272*, 22182−22190.
49. Minami, H., Tokumitsu, H., Mizutani, A., Watanabe, M., and Hidaka, H. (1992) *FEBS Lett. 305*, 217−219.
50. Guex, N., and Peitsch, M. C. (1997) *Electrophoresis 18*, 2714−2723.
51. Brünger, A. T. (1993) *Acta Crystallogr., Sect. D D49*, 24−36.

BI002507S